Indian Journal of Pure & Applied Physics
Vol. 55, November 2017, pp. 829-835

Synthesis and characterization of hybrid solar cell based on zinc blend semiconductor quantum dots

Harit Kumar Sharma* & S L Agrawal
Department of Physics, A P S University, Rewa 486 003, India

Received 15 March 2017; accepted 7 June 2017

An attempt have been made to synthesise and characterize of undoped and doped zinc blend based semiconducting quantum dots prepared by a simple wet chemical precipitation method for solar cell application. Formation of semiconducting quantum dot has been ascertained by X-ray diffraction (XRD), UV-visible spectroscopy, transmission electron microscopy (TEM) and impedance spectroscopy measurements. XRD studies confirm that all the prepared samples are in zinc-blende phase and in quantum dot regime. Dopants copper and cadmium cause a shift in diffraction peaks towards lower diffraction angles with linear increase in lattice constant values. UV-visible studies reveal decrease in optical bandgap of the QDs with co-doping of Cd and Cu ion in ZnS lattice though bandgap energy is higher than that of corresponding bulk material due to quantum confinement effect and alloyed formation of nanoparticles. TEM pictures reaffirm nanocrystalline nature of samples with size ranging 4 to 8 nm supporting XRD result. Mott-Schottky analysis revealed *n*-type conductivity of as prepared semiconducting QDs. To test the utility of these materials bulk heterojunction hybrid solar cells have been fabricated in 1 cm×1 cm size with *p*-type polypyrrole. Solar cells with quaternary zinc blend $\{(Zn_{0.85}Cu_{0.15})_{0.5}Cd_{0.5}S\}$ structure under AM 1.5 illumination resulted in highest conversion efficiency of 1.8% and fill factor 0.81.

Keywords: Hybrid solar cell, Doctor's blade technique, Zinc blend based semiconductor

1 Introduction

Among the existing solar cell technologies, Hybrid solar cells represent a new stage in the evolution of photovoltaic devices, and as suggested by the name, it involves the blending of inorganic and organic material to form a solar cell[1,2]. Various combinations of inorganic semiconductors and organic conducting polymers have been looked upon as probable candidates for hybrid photovoltaic materials. Among the electron acceptors, CdS[3], CdSe[4], CdTe[5], PbS[6], ZnO[7,8] and TiO_2[9] etc., have been attempted thus far, while more choices are available for conducting polymers. It is worth emphasising here that the charge generation is principally governed by the energy-level alignment at the donor/acceptor interfaces, but the photocurrent in the final device depends on the appropriate energy level alignment at the electrode interfaces. This has prompted researchers to find good combination to deliver high conversion efficiency in solar cells. To obtain high efficiencies in bulk heterojunction solar cells, it is necessary to have an interpenetrating network of electron-accepting and hole-accepting components within the device which are achieved using conjugated polymers blends or a mixture of conjugated polymers with C_{60} derivatives[10]. Similarly, Group II–VI semiconducting materials are good candidates for use in such solar cells. Among the II-VI group, inorganic materials reported thus for ZnS appears to be a favourable candidate for development of hybrid solar cells owing to its distinctive optoelectronic properties[11-13]. However its usage in solar cell application has been hindered owing to large band gaps. A strategy has been adopted in present work to reduce its band gap by doping with compounds of Cd and Cu to make ternary and quaternary composition because tunable optical band gap plays a major role to synthesize efficient solar cells[14]. Such structures might lead to enhancement in photon absorption thereby causing improvement in conversion efficiency of solar cells[15,16]. In view of the above, making ternary and quaternary ZnS nanopowders have been synthesized and characterized using co-precipitation method. Subsequently hybrid solar cells have been fabricated with *p*-type polypyrrole followed by its performance study to explore their utility in solar cell applications.

2 Experimental Details

Appropriate molar amount of zinc acetate, cadmium acetate, copper acetate and sodium sulphide

*Corresponding author (E-mail: haritsharma2@gmail.com)

were taken as precursor salts in the synthesis of ZnS, $Zn_{0.5}Cd_{0.5}S$ and $(Zn_{0.85}Cu_{0.15})_{0.5}Cd_{0.5}S$ nanopowders employing co-precipitation technique. In the first step, three different solutions of zinc acetate dehydrate, cadmium acetate dehydrate and cupric acetate dissolved separately in appropriate amount of methanol were admixed such that mixture solution I is 0.1 mol. Similarly, a saturated solution of sodium sulphide fused flakes termed solution II was prepared by dissolving Na_2S in 0.1 mol in methanol. In the second step, firstly solution I was vigorously stirred using a magnetic stirrer for 30 min, and then solution II was added to solution I drop wise till pH of the solution becomes 8. The overall mixed solution has further stirred for 1 h to complete the chemical reaction. The resulting precipitates were filtered several times with methanol to remove impurities and dried at room temperature. X-ray studies were conducted on Shimadzu make X-ray diffractometer (model 2203) in 2θ range 20 °C to 70 °C having Cuk_{α} radiation wavelength 1.5406 Å. Band gap and particle size of all the samples were estimated from UV-Vis data obtained with the help of Systronics make UV-Visible spectrophotometer (model 2203) in 200 nm-1100 nm wavelength range. TEM images of all synthesized semiconducting QD's were recorded on JEOL JXA-810 instrument at 200 KV. Mott-Schottky analysis was carried out with the help of LCR meter (Hioki Japan make model 3520). With these nanopowders and as synthesized *p*-type polypyrrole a bulk hetero junction solar cell was fabricated employing doctor's blading technique. Electrical characterization was performed using a computer-controlled Keithley 2400 Source Meter in the dark and under illumination to assess performance of fabricated solar cells. The photovoltaic devices were illuminated using a metal-halide lamp calibrated to an intensity of 1 kW/m^2 (in accordance with standard testing conditions AM 1.5G). All measurements were performed at a constant temperature of 295 K (room temperature) and the temperature of the device was kept constant.

3 Results and Discussion

3.1 Structural analysis

Figure 1 shows the X-ray diffraction patterns of ZnS, $Zn_{0.5}Cd_{0.5}S$ and $(Zn_{0.85}Cu_{0.15})_{0.5}Cd_{0.5}S$ semiconductor nanoparticles. The characteristic XRD patterns of ZnS QD'S exhibited three prominent peaks 2θ = 28.54°, 47.62°, 56.28° which correspond to (111), (220), and (311) planes of the cubic phase of ZnS with lattice constant a=5.4 Å (JCPDS card No. 05-0566). No peaks for any impurity phase or metallic clustering were observed. All these peaks are apparent even in XRD patterns of $Zn_{0.5}Cd_{0.5}S$ and $(Zn_{0.85}Cu_{0.15})_{0.5}Cd_{0.5}S$ powder but with gradual shift towards lower diffraction angles upon incorporation of Cd in ZnS lattice and as well as co-doping the resulting system with Cu. With doping of Cd concentration and Cu concentration, continuous peak shifting of the nanoparticles suggests a successful formation of alloyed nanoparticles because of the small difference in the bond length of ZnS, CdS and Cu_2S and very close electronegativity value of Cd and Zn which allows the formation of their solid-solution. The estimated crystallite size of the synthesized nanopowders have been summarised in Table 1. It can be seen from Fig. 1 that there is only a marginal shift in the XRD peak position toward lower angle with doping of Cu concentration but with enhanced broadening of corresponding peaks. According to Hume Rothary rules[17] for the formation of substitutional solid solutions, the ionic radii of the solute and solvent atoms must not differ by more than 15%. In the present case ionic radii difference is around ~ 2.7% satisfying the condition set by this. This helps to rule out the possibility of "Cu" ions coming out of the host lattice. Thus, one can easily conclude that substitutional Cu-doping in $Zn_{1-x}CdxS$ lattice has been accomplished. The XRD peaks are broadened due to nanocrystalline nature of the synthesized samples. The crystallite size corresponding to the observed Zinc blend based semiconducting quantum dots peaks have been calculated from the Debye- Scherrer relation[18]:

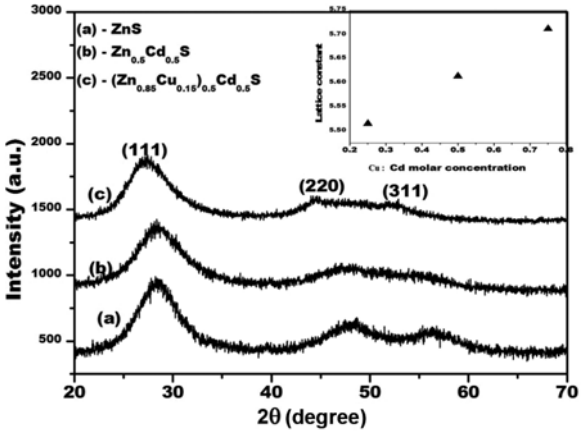

Fig. 1 — XRD graph of zinc blend based semiconducting quantum dots.

Table 1 — XRD table of Zinc blend based semiconducting quantum dots.

Sample description	Angle 2θ (degree)	*d*-spacing (Å)	Identified Possible *h k l* planes	Average crystallite size by Scherrer's formula (nm)	Average particle size from TEM images (nm)	*W-H* plot	
						Strain	Effective crystallite size
	28.54	3.1250	1 1 1				
ZnS	47.62	1.9080	2 2 0	~ 3.5	~ 4	-0.051	2.2
	56.28	1.6332	3 1 1				
	26.50	3.3608	1 1 1				
$Zn_{0.5}Cd_{0.5}S$	43.95	2.0582	2 2 0	~ 4.8	~ 6	-0.052	3.8
	52.15	1.7523	3 1 1				
	26.42	3.3693	1 1 1				
$(Zn_{0.85}Cu_{0.15})_{0.50}Cd_{0.5}S$	43.32	2.0621	2 2 0	~ 6.5	~ 8	-0.054	6.6
	51.62	1.7692	3 1 1				

$$D = \frac{0.9\lambda}{\beta\cos\theta} \quad \ldots (1)$$

where, λ is the wave length (Å) of the X-rays, β is the full width at half maximum (FWHM) in radians, θ is the Bragg angle and *D* is the mean size of crystallites. The estimated crystallite sizes of the synthesized nanoparticles have been listed in Table 1. From the table it is apparent that crystallites size of synthesised nanopowders fall in quantum dot regime and it increases with doping of Cu and Cd.

In order to check whether lattice imperfections are present in synthesized samples, strain from the XRD pattern was also calculated using well known Williamson-Hall method[19]. Figure 2 displays the Williamson-Hall plot for ZnS and its ternary and quarternary studies synthesised in the laboratory. Calculated values of local strain and particle size of all samples from these plots are also shown in Table 1. Magnitude of local strain increases, as expected, with dopants and presents compressive strain (negative value of strain). Despite these variations particle sizes remain in nano regime.

Semiconductor alloys solid solutions have known to follow Vegard's law[20], revealing the linear relationship between the lattice constant and composition as follows:

$$a^0\, A_{1-x}B_xC(x) = (1-x)a^0_{AC} + x \quad \ldots (2)$$

where $a^0\, A_{1-x}B_xC(x)$ is the natural constant of the ternary form $a^0\, A_{1-x}B_xC(x)$ and a^0_{AC} and a^0_{BC} are the natural constants of the binaries AC and BC, respectively, and *x* is the mole fraction of binary BC. As shown in inset of Fig. 1, lattice constants of ZnS appears to increase linearly with dopant concentration, where cubic $a^0_{ZnS} = 5.4060$ Å (PDF # 05-0566) and $a^0_{CdS} = 5.820$ Å (PDF #01-0647)

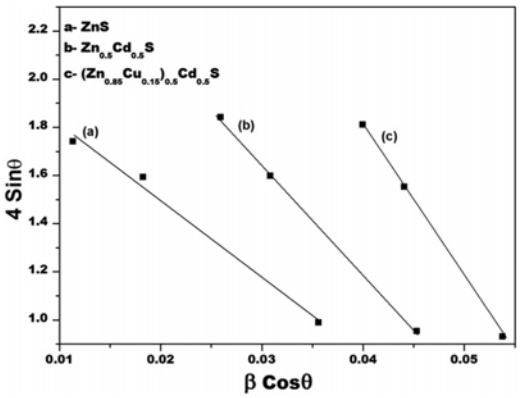

Fig. 2 — *W-H* plot of zinc blend based semiconductor quantum dots.

and $a^{\circ}_{Cu_2S} = 5.628$ Å (PDF $\neq 05-0545$) values have been taken for calculation of ternary and quaternary composition of ZnS. These observations indicate that the composition of the alloy was very close to the mixing molar ratio of the starting materials.

3.2 Surface morphological studies

Figure 3(a) depicts the bright field TEM graphs of ZnS which shows crystalline aggregates of ZnS resulting from fine and spherical nanoparticles. As shown, the ZnS particles are uniform in size, with diameter lying in the range ~4 nm. TEM graph of $Zn_{0.5}Cd_{0.5}S$ nanopowder also shows the uniform distribution of nanoparticles spherical in shape and size lying between ~6 nm. Quaternary composition $(Zn_{0.\ 85}Cu_{0.15})_{0.5}Cd_{0.5}S$ too exists spherical shape with smooth surface in its TEM image (Fig. 3(c)). The particle size of $(Zn_{0.85}Cu_{0.15})_{0.5}Cd_{0.25}S$ is estimated to about ~ 8 nm in diameter.

3.3 Optical studies

The optical absorption characteristics of ZnS, $Zn_{0.5}Cd_{0.5}S$ & $(Zn_{0.85}Cu_{0.15})_{0.5}Cd_{0.5}S$ samples were

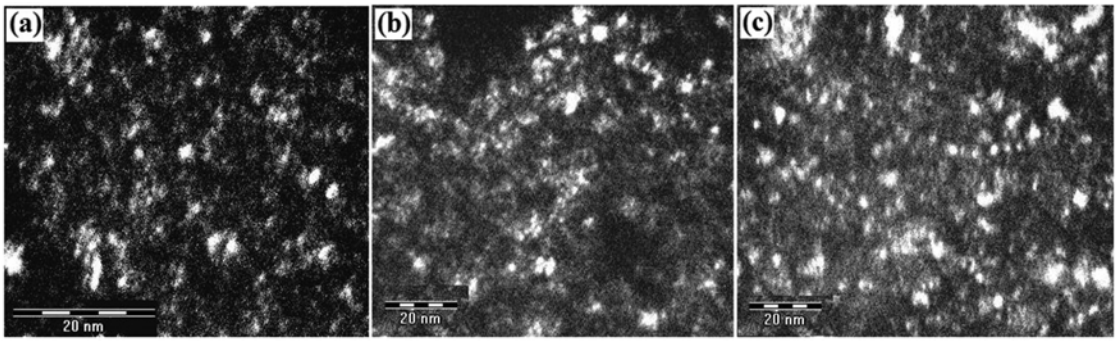

Fig. 3 —TEM graph of (a) ZnS, (b) $Zn_{0.5}Cd_{0.5}S$ and (c) $(Zn_{0.85}Cu_{0.15})_{0.5}Cd_{0.5}S$ semiconducting quantum dots.

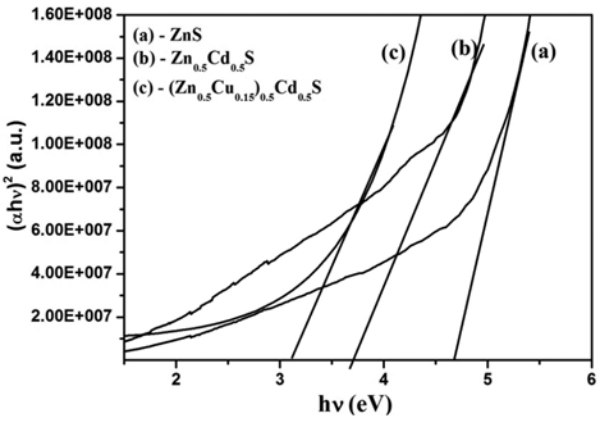

Fig. 4 — Tauc's plot for the determination of optical bandgap of zinc blend based semiconducting quantum dots.

recorded to estimate there band gap energies in the wavelength range of 200-1100 nm. Band gap (E_g) of the material is related by the well known Tauc's relation[21,22]:

$$(\alpha h\nu) = K(h\nu - E_g)^n \quad \ldots (3)$$

where K is the edge width parameter, $h\nu$ the incident photon energy and parameter n depends on the type of transition, i.e., allowed direct, allowed indirect, forbidden direct and forbidden indirect for which it can have value ½, 2, 3/2, and 3, respectively. Thus the direct band gap of ZnS, $Zn_{0.5}Cd_{0.5}S$ & $(Zn_{0.85}Cu_{0.15})_{0.5}Cd_{0.5}S$ nanoparticles was calculated by plotting a graph between $(\alpha h\nu)^2$ versus $h\nu$ as shown in Fig. 4 and extrapolating the straight line portion of the graph (showing the maximum transmission, i.e., $\alpha = 0$) on the $h\nu$ axis. Band gap values so obtained have been listed in Table 2. It is apparent from the table that band gap of ZnS nanoparticles decreases with the doping of Cd and Cu ions. This red shift of band gap can be attributed to quantum confinement effect as well as the doping of Cd and Cu ions in ZnS lattice.

Table 2 — Optical band gap of zinc blend based quantum dots.

Sample description	Optical band gap (eV)	Composition dependent nano band gap	Quantum confinement effect dependent band gap
ZnS	4.5	3.60	4.48
$Zn_{0.50}Cd_{0.50}S$	3.6	2.87	3.67
$(Zn_{0.85}Cu_{0.15})_{0.5}Cd_{0.5}S$	3.1	2.994	2.883

In the case of alloyed nanoparticles, the bandgap energies are determined by their size and composition, i.e., quantum confinement effect and alloying effect. The bulk band gap energy in case of ternary composition of ZnS (i.e., $Zn_{0.5}Cd_{0.5}S$) can be obtained from the empirical relation[12,13] given by:

$$E_{g(x)} = E_g(\mathrm{ZnS}) + \left[E_g(\mathrm{CdS}) - E_g(\mathrm{ZnS}) - b\right]x + bx^2 \quad \ldots (4)$$

where E_g(ZnS) and E_g(CdS) are the band gap energies for bulk ZnS and CdS, respectively, and b is the bowing parameter which has[12,13] the value 0.61. Using the bulk band gap energy values of ZnS as 3.6 eV and of CdS as 2.36 eV, band gap of $Zn_{0.5}Cd_{0.5}S$ nanoparticles with the average size of 3.36 nm, (Table 1) band gap energy was estimated as 2.87 eV in accordance with Eq. (4). In quaternary composition, i.e., $(Zn_{0.85}Cu_{0.15})_{0.5}Cd_{0.5}S$ sample the bandgap energy was estimated from an empirical relation analogous to Eq. (4). This modified relation can be expressed as:

$$E_{g(x)} = E_g\left(\mathrm{Zn_{(1-x)}Cd_{(x)}S}\right) + \left[E_g(\mathrm{Cu_2S}) - E_g\left(\mathrm{Zn_{(1-x)}Cd_{(x)}S}\right) - b\right]x + bx^2 \quad \ldots (5)$$

The calculated band gap values for $Zn_{0.5}Cd_{0.5}S$ and $(Zn_{0.85}Cu_{0.15})_{0.5}Cd_{0.5}S$ sample have been given in Table 2.

The fundamental bandgap of the nanoparticles due to quantum confinement effects (QCE) is well established[12,13] and is given by the relation:

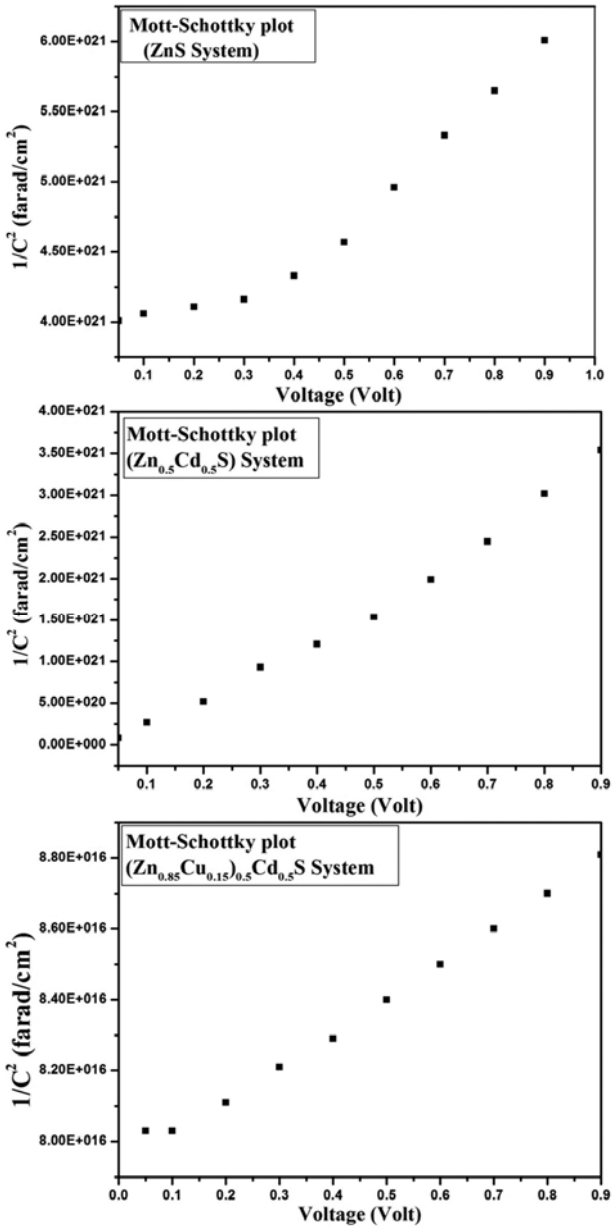

Fig. 5 — Mott-Schottky plot of zinc blend based semiconducting quantum dots.

$$E_g = E_g^0 + \frac{h^2}{8\mu R^2} - \frac{1.8e^2}{4\pi\varepsilon R} \quad \text{... (6)}$$

where E_g^0 is the energy band gap in for the bulk material, R is the radius of the nanoparticle calculated from XRD data, $1/\mu = 1/m_e + 1/m_h$ (m_e and m_h being the electron and hole effective masses, respectively), ε the dielectric constant and e the electronic charge. The experimental values of the dielectric constant for ZnS and CdS used in present study are 4.2 and 5.5, respectively. Similarly effective mass of electrons and holes for ZnS and CdS are 0.25 m_0, 0.51 m_0 and 0.19 m_0, 0.8 m_0, respectively. On substituting all these values in Eq. (6), size dependent bandgap energy relations for ZnS and CdS are derived for quantum confined structure and can be expressed as:

$$E_g = E_g^0 + 5.237R^{-2}(\text{nm})\text{-}0.61R^{-1}(\text{nm}) \quad \text{... (7)}$$

$$E_g = E_g^0 + 4.784R^{-2}(\text{nm}) - 0.832R^{-1}(\text{nm}) \quad \text{... (8)}$$

Taking average particle size of 2.5 nm for ZnS and CdS 3.2 nm (Table 1) a shift in the band gap values of 0.88 and 0.51 eV is obtained for ZnS and CdS, respectively. It should be noted that dielectric constant of Cu_2S in 4.5. Since there is no appreciable difference between the dielectric constant values of ZnS, CdS and Cu_2S, an average value ε(x) = 4.5 can be taken for quaternary composition, in the calculation of band gap based on quantum confinement. By substituting all the values (particle size, dielectric constant and effective mass) in Eq. (6), size dependent bandgap energy relations for $Zn_{1-x}Cd_xS$ (x=0.5 M) and Cu_2S is derived. Corresponding equations for $Zn_{1-x}Cd_xS$ and Cu_2S are:

$$E_g = E_g^0 + 2.51R^{-2}(\text{nm}) - 0.349R^{-1}(\text{nm}) \quad \text{... (9)}$$

$$E_g = E_g^0 + 5.95R^{-2}(\text{nm}) - 0.577R^{-1}(\text{nm}) \quad \text{... (10)}$$

Taking average particle size of quaternary sample (XRD data; Table 1), a shift in the band gap values was obtained for $(Zn_{0.85}Cu_{0.15})_{0.5}Cd_{0.5}S$. From Table 2, energy band gap values of Zinc blend samples reveal role of both alloying and quantum confinement effect and the values agree well with the value obtained experimentally.

3.4 Mott-Schottky study

Mott-Schottky plots were drawn (under dark conditions) to evaluate the semiconductor parameters at a frequency of 1 kHz for ZnS, $Zn_{0.5}Cd_{0.5}S$ & $(Zn_{0.85}Cu_{0.15})_{0.5}Cd_{0.5}S$ samples as shown in Fig. 5. The value of flat band potential (V_{fb}) was obtained making use of relation[23,24]:

$$\frac{1}{C_{sc}^2} = (V - V_{fb} - \frac{k_B T}{e}).\frac{2}{\epsilon\epsilon_0 A^2 e N_d} \quad \text{... (11)}$$

where ϵ_0 is the dielectric constant of free space (8.854×10^{-12} F/m), ε the dielectric constant of samples, e the electronic charge (1.603×10^{-19} C), A is area such that the depletion region volume is ωA and N_D the doping density, and calculated from the slope of the graph. T the temperature of the operation

Table 3 — Mott-Schottky plot data and solar cell parameters of zinc blend based quantum dots.

Sample description	Mott-Schottky characterisation			Hybrid solar cell characterisation	
	Doping density (N_D) (cm^{-3})	Flat band potential f_b(V)	Type of conduction	Fill factor	PCE (%)
ZnS	11.2×10^{20}	0.248	N	0.22	0.1
$Zn_{0.5}Cd_{0.5}S$	3.3×10^{21}	0.112	N	0.38	1.6
$(Zn_{0.85}Cu_{0.15})_{0.5}Cd_{0.5}S$	1.677×10^{24}	0.044	N	0.81	1.8

(300 K), K_B is the Boltzmann's constant (1.38×10^{-23} J/K), and C_{sc} is the space charge capacitance. The positive slope of the Mott-Schottky plot reconfirms *n*-type conductivity behaviour of synthesised zinc blend structures. Among the different compositions of zinc blend structures it is clear from Table 3 and the data presented in Fig. 5(a,b,c), that Mott-Schottky equation is valid within a wide potential range, of about ~ 0.24 V, which indicates a well-defined electronic surface state of zinc blend based samples. Also the donor concentration in quaternary structure increases with respect to binary zinc blende (Table 3).

3.5 Solar cell characteristic study

The performance of a photovoltaic device is determined by measuring its current–voltage characteristics and so electrical characterization was performed. The current response was measured in the voltage range -1 V to +1 V. *I-V* characteristics for fabricated hetero junction devices built around Polypyrrole/ZnS, Polypyrrole/ $Zn_{0.5}Cd_{0.5}S$ and polypyrrole/$(Zn_{0.85}Cu_{0.15})_{0.5}Cd_{0.5}S$ under dark and under illumination condition are shown in Fig. 6, respectively. The *I-V* characteristics of as prepared hybrid hetero junction devices shows diode characteristics behaviour both under dark and illuminated condition confirming formation of hybrid solar cell. Further magnitude of current enhances in the device as the composition of acceptor material changes from binary to ternary to quaternary. Figure 7 shows the photo response curve of solar cells with respect to variation in voltage. Table 3 also depicts different solar cell parameters of as synthesised hybrid solar cells. From these results, one finds that conversion efficiency of polypyrrole/ZnS cell is not adequate. This can be attributed to the fact that ZnS being wide band gap semiconductor there is improper band alignment between polypyrrole and ZnS which in turn causes inefficient excition dissociation and thus less efficient solar device formation. On the other hand, the devices with polypyrrole[25] / $Zn_{0.5}Cd_{0.5}S$ and polypyrrole/$(Zn_{0.85}Cu_{0.15})_{0.5}Cd_{0.25}S$ are efficient. It can be expected that cell efficiency of polypyrrole/ $Zn_{0.5}Cd_{0.5}S$ and polypyrrole /$(Zn_{0.85}Cu_{0.15})_{0.5}Cd_{0.5}S$ results from

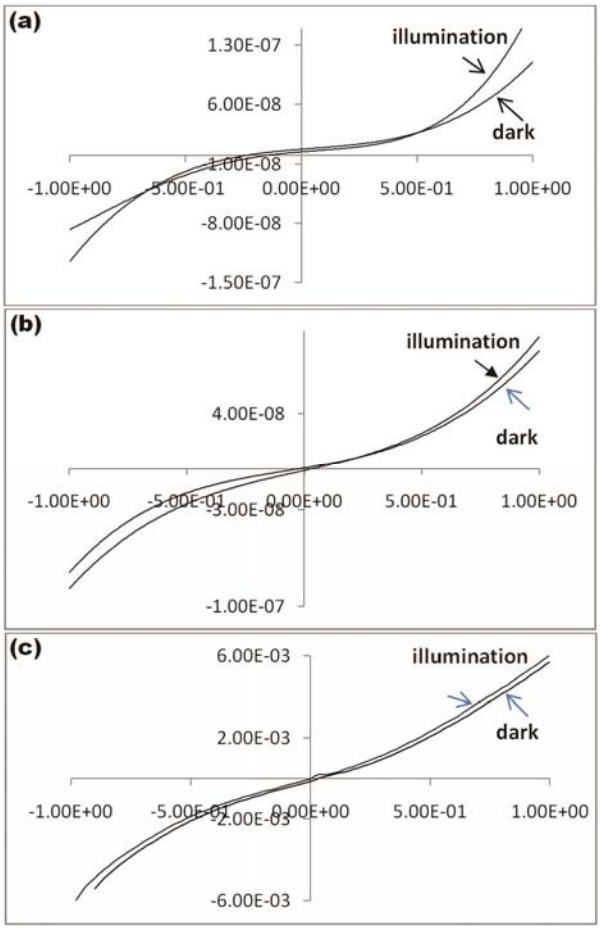

Fig. 6 — *I-V* graph of (a) ZnS/ Ppy, (b) $Zn_{0.5}Cd_{0.5}S$/Ppy and (c) $(Zn_{0.85}Cu_{0.15})_{0.5}Cd_{0.5}S$/Ppyhybrid solar cell samples under dark and illumination condition.

the good charge balance of hole and electron at the interface and the formation of a well-ordered morphology. The reason of dramatically increase in efficiency could be attributed to the possibility that energy transfer rather than charge transfer could occur from the donor (polypyrrole) to acceptor (using ternary and quaternary QD's) in polypyrrole/$Zn_{0.5}Cd_{0.5}S$ and polypyrrole/$(Zn_{0.85}Cu_{0.15})_{0.5}Cd_{0.5}S$ blends, resulting in a sufficient generation of free charge carriers. Best conversion efficiency and fill factor was achieved for hybrid solar cells designed around quaternary composition of ZnS.

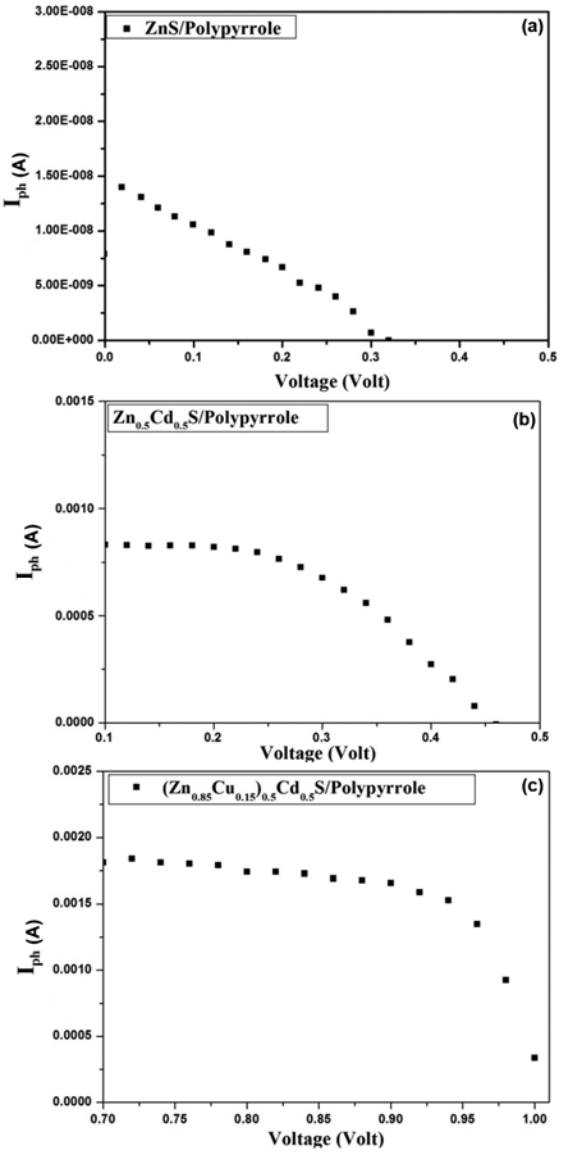

Fig. 7 — (a) I_{ph} versus V graph ZnS/polypyrrole hybrid solar cell, (b) I_{ph} versus V graph of $Zn_{0.5}Cds_{0.5}S$/polypyrrole hybrid solar cell and (c) I_{ph} versus V graph of $(Zn_{0.85}Cu_{0.15})_{0.5}Cd_{0.5}S$/polypyrrole hybrid solar cell.

4 Conclusions

For the preparation of hybrid bulk hetero junction solar cell, zinc blend based semiconducting quantum dots with co-doping of Cd and Cu are synthesized by simple wet chemical co-precipitation method without using any capping agent. X-ray diffraction study confirmed proper cubic phase formation. Red-shift in optical band gap spectra results from quantum confinement effect and formation of alloyed nanoparticles. TEM diffraction patterns confirm X-ray diffraction predictions about particle size viz, 4-8 nm. No signature of Cu_2S or other impurity phases are found in our samples. From the Mott-Schottky plot, the semiconductor parameters were determined with *n*-type semiconducting nature of synthesised nanoparticles with highest doping concentration for quaternary composition. The characterization and findings on hybrid solar cell designed around inorganic semiconducting QD's and polymeric semiconductor shows better photo response with quaternary quantum dots with highest conversion efficiency of 1.8% and fill factor 0.81. Present studies reveal importance of II-VI group of semiconductor in design and performance of hybrid solar cell structure.

References

1 Choi K C, Lee E J, Baek Y K, Lim D C, Kang K C & Kim Y D, *Electron Acta*, 180 (2015) 435.
2 Nelson J, *The physics of solar cells*, 1st Edn. (Imperial College Press), 2003.
3 Cao X, Wang N & Kim X, *Electrochim Acta*, 56 (2011) 9504.
4 Schierhorn M, Boettcher S W, Peet J H, Matioli E, Bazan G C, Stucky G D & Moskovits M, *Acs Nano*, 4 (2010) 6132.
5 Fan Z X, Zhang H, Yu W L, Xing Z Y, Wei H T, Dong Q F, Tian W J & Yang B, *ACS Appl Mater Interfaces*, 3 (2011) 2919.
6 Seo J, Kim S J, Kim W J, Singh R, Samoc M, Cartwright A N & Prasad P N, *Nanotechnology*, 20 (2009) 20.
7 Noori K & Giustino F, *Adv Funct Mater*, 22 (2012) 5089.
8 Sung Y H, Liao W P, Chen D W, Wu C T, Chang G J & Wu J J, *Adv Funct Mater*, 22 (2012) 3808.
9 Ozdal T, Hames Y & Aslan E, *Appl Surf Sci*, 258 (2012) 5259.
10 Li G, Zhu R & Yang Y, *Nature Photonics*, 6 (2012) 11.
11 Sharma H K, Shukla P K & Agrawal S L, *J Optoelectron Adv Mater*, 17 (2015) 608.
12 Sharma H K, *Int J Eng Sci Res Technol*, 5 (2016) 921.
13 Sharma H K, Shukla P K & Agrawal S L, *J Mater Sci Mater Electron*, 28 (2017) 6226.
14 Ji LW, Hsiao Y J, Tang I T, Meen T H, Liu C H, Tsai J K, Wu T C & Wu Y S, *Nanoscale Res Lett*, 8 (2013) 470.
15 Mohapatra J K, *Int Nano Lett*, 3 (2013) 31.
16 Chawala A K, Singhal S, Gupta H O & Chandra R, *Curr Nanosci*, 6 (2010) 94.
17 Tsai A P, *J Non Cryst Solids*, 317 (2004) 334.
18 Cullity B D, *Elements of X-ray diffraction*, (Addison Wesley Co: USA), 1978.
19 Kole A K & Kumbhakar P, *Res Phys*, 2 (2012) 150.
20 Singh J, *Optoelectronics an introduction to materials and devices*, (Macgraw Hill: New Delhi), 1996.
21 Skoog A, Douglas F, Holler C, James R & Stanley, *Principles of instrumental analysis*, (6th Edn). (Belmont, CA: Thomson Brooks/Cole), (2007) 169.
22 Sze S M, *Physics of semiconductor devices*, (Wiley: New York), 1969.
23 Gupta R K & Singh R A, *Mater Sci Semicond Process*, 7 (2004) 83.
24 Saxena V & Santhanam K S V, *Curr Appl Phys*, 3 (2003) 227.
25 Sharma H K, Pandey S K & Agrawal S L, *J Phys Conf Ser*, 836 (2017) 012054.